Front. Environ. Sci. Eng. 2022, 16(11): 139
https://doi.org/10.1007/s11783-022-1574-z

RESEARCH ARTICLE

Variation characteristics of atmospheric methane and carbon dioxide in summertime at a coastal site in the South China Sea

Yangyan Cheng[1,2,5], Ye Shan[3], Yuhuan Xue[1,2,5], Yujiao Zhu[3], Xinfeng Wang[3], Likun Xue[3], Yanguang Liu[4], Fangli Qiao[1,2,5], Min Zhang (✉)[1,2,5]

1 Key Laboratory of Marine Sciences and Numerical Modeling, First Institute of Oceanography, Ministry of Natural Resources, Qingdao 266061, China
2 Laboratory for Regional Oceanography and Numerical Modeling, Pilot National Laboratory for Marine Science and Technology (Qingdao), Qingdao 266237, China
3 Environment Research Institute, Shandong University, Qingdao 266237, China
4 Key Laboratory of Marine Geology and Metallogeny, First Institute of Oceanography, Ministry of Natural Resources, Qingdao 266061, China
5 Shandong Key Laboratory of Marine Sciences and Numerical Modeling, Qingdao 266061, China

HIGHLIGHTS

- Diurnal patterns of CH_4 and CO_2 are clearly extracted using EEMD.
- CH_4 and CO_2 show mid-morning high and evening low patterns during sea breezes.
- Wind direction significantly modulates the diurnal variations in CH_4 and CO_2.

GRAPHIC ABSTRACT

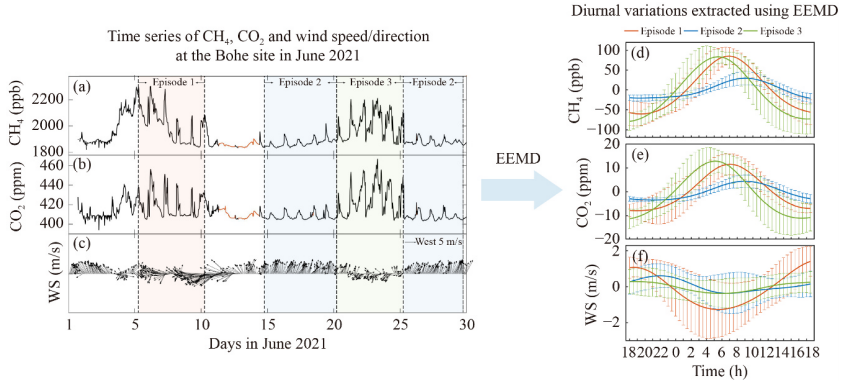

ARTICLE INFO

Article history:
Received 10 November 2021
Revised 5 April 2022
Accepted 10 April 2022
Available online 13 May 2022

Keywords:
Methane
Carbon dioxide
Diurnal pattern
Ensemble empirical mode decomposition
South China Sea
Sea breeze

ABSTRACT

Methane (CH_4) and carbon dioxide (CO_2) are the two most important greenhouse gases (GHGs). To examine the variation characteristics of CH_4 and CO_2 in the coastal South China Sea, atmospheric CH_4 and CO_2 measurements were performed in Bohe (BH), Guangdong, China, in summer 2021. By using an adaptive data analysis method, the diurnal patterns of CH_4 and CO_2 were clearly extracted and analysed in relation to the sea breeze (SB) and land breeze (LB), respectively. The average concentrations of CH_4 and CO_2 were 1876.91 ± 31.13 ppb and 407.99 ± 4.24 ppm during SB, and 1988.12 ± 109.92 ppb and 421.54 ± 14.89 ppm during LB, respectively. The values of CH_4 and CO_2 during SB basically coincided with the values and trends of marine background sites, showing that the BH station could serve as an ideal site for background GHG monitoring and dynamic analysis. The extracted diurnal variations in CH_4 and CO_2 showed sunrise high and sunset low patterns (with peaks at 5:00–7:00) during LB but mid-morning high and evening low patterns (with peaks at 9:00) during SB. The diurnal amplitude changes in both CH_4 and CO_2 during LB were almost two to three times those during SB. Wind direction significantly modulated the diurnal variations in CH_4 and CO_2. The results in this study provide a new way to examine the variations in GHGs on different timescales and can also help us gain a better understanding of GHG sources and distributions in the South China Sea.

1 Introduction

Carbon dioxide (CO_2) and methane (CH_4) are the two most important greenhouse gases (GHGs) in the

✉ Corresponding author
E-mail: zhangmin@fio.org.cn

atmosphere and are directly linked to global warming and climate change. CO_2 and CH_4 comprise less than 0.04% in the atmosphere but contribute more than 80% (66% for CO_2 and 16% for CH_4) of the increase in global radiative forcing of long-lived greenhouse gases since the preindustrial era (World Meteorological Organization, 2020). The two main sources of atmospheric CO_2 are the burning of fossil fuels and changes in land use, while CH_4 has large emissions from both natural (e.g., wetlands and geological processes) and anthropogenic origins (e.g., fossil fuels, agriculture and waste treatment) (Saunois et al., 2016; Canadell et al., 2021; Bai et al., 2022). During the 1750–2019 period, atmospheric CO_2 and CH_4 increased by 47.3% and 157.8%, respectively, reaching unprecedented levels during at least the past 800000 years, while global surface temperature also substantially increased by 1.09 °C from 1850–1900 to 2011–2020, which is mostly attributed to anthropogenic emissions (Gulev et al., 2021). In addition, more CO_2 and CH_4 could be released into the atmosphere under a warmer climate (Li et al., 2021). Subsequently, the frequency and intensity of extreme climate events have dramatically increased, with high potential impacts on both ecosystems and human society (Coumou and Rahmstorf, 2012; Diffenbaugh et al., 2016).

The fast increase in atmospheric CH_4 from both observations and prediction models has become a threat to the surface heat balance of the Earth (Clow and Smith, 2016). Looking 100 years into the future, the global warming potential (GWP) value of CH_4 is approximately 28 times greater than CO_2 for global warming on an equivalent concentration basis (Forster et al., 2021). The mean lifetime of CH_4 is approximately 12 years, and by chemical reactions, approximately 90% of CH_4 finally generates ground-level ozone, an air pollutant harmful to human health (Zhang et al., 2014; Saunois et al., 2016; Zhang et al., 2020). Therefore, reducing anthropogenic CH_4 emissions is an effective way to mitigate global warming and simultaneously improve air quality (Dlugokencky et al., 2011; Kavitha et al., 2018). It is predicted that if human-caused CH_4 emissions could be reduced by as much as 45% by 2030, nearly 0.3 °C of global warming over the next two decades would be successfully avoided (United Nations Environment Programme, 2021).

Within the networks of the World Meteorological Organization/Global Atmosphere Watch (WMO/GAW) program, surface CO_2 and CH_4 concentrations have been monitored globally since the late 1960s and late 1970s, respectively (Dlugokencky et al., 2011). Ship-borne measurements of atmospheric CO_2 and CH_4 are also conducted in different seas/oceans (Zang et al., 2013; Zhang et al., 2017). To date, many coastal areas, which are important sources for climatically active trace gases, are still greatly undersampled for GHGs (Cai et al., 2006; Kong et al., 2010; Ji et al., 2017). There have been many studies on the changes in atmospheric CO_2 and CH_4 in urban and suburban China (e.g., Mt. Waliguan and Longfengshan stations in China) (Fang et al., 2017). The South China Sea (SCS), as the largest deep marginal sea in the western Pacific Ocean, is situated at the confluence of the tropical Indian and Pacific Oceans with a maximum water depth over 5000 m, which is of both great significance to climate and strategies (Qu et al., 2009). To date, limited in situ measurements of atmospheric CO_2 and CH_4 in the SCS are available (Lv et al., 2015; Jiang et al., 2021), but the direct measurements of CO_2 and CH_4 are still largely insufficient in the coastal SCS.

The diurnal patterns of CO_2 and CH_4 are characterized by unimodal distributions, with peak values at 5:00–7:00 local time and the lowest values appearing during the daytime at approximately 13:00–15:00 for most observations (Lv et al., 2015; Kavitha et al., 2018; Wei et al., 2019; Dimitriou et al., 2021; Jiang et al., 2021). The observations on Yongxing Island (China) are an exception, with peak values of CH_4 occurring at approximately 23:00–00:00 (Jiang et al., 2021). The diurnal patterns of CO_2 and CH_4 are mainly determined by the following factors: 1) the variations in boundary layer height (BLH) lead to the compression and dilution of trace gases; 2) photochemical reactions with other atmospheric components lead to production or deletion; 3) changes in wind directions are accompanied by changes in air masses; and 4) other local emission sources and industrial activities (Srivastava et al., 2010; Thomas and Zachariah, 2012; Kavitha et al., 2018). Although with different influencing factors, the diurnal patterns reported in previous studies at different observational sites with different emission sources are almost similar, and the diurnal pattern of the BLH could be one of the determining factors. However, for coastal sites, the impact of wind directions, such as land breezes (LB) or sea breezes (SB), can not be ignored and may even be a determining factor for diurnal variations in CO_2 and CH_4 (Kavitha et al., 2018; Wei et al., 2019).

Traditionally, previous studies have extracted and examined the diurnal patterns of CO_2 and CH_4 by intercepting the original signals every 24 hours, and then simply averaging all 24-hour data fragments (Lv et al., 2015; Kavitha et al., 2018; Wei et al., 2019; Dimitriou et al., 2021; Jiang et al., 2021). These methods, which take the running mean of the traditional diurnal cycle, share the assumption that the time series is stationary and quasi-stationary. However, as CO_2 and CH_4 vary on all timescales simultaneously, their intercepted 24-hour data fragments generally include information for all timescales. In addition, the diurnal variation in each day, as a nonlinear process, could vary with time and location. When extracting the diurnal patterns, simply averaging without signal screening could obscure the intrinsic diurnal variations. The ensemble empirical mode

decomposition (EEMD) method provides a new way to study the phenomena on different timescales by effectively extracting the signals on different timescales from original timeseries for both linear and nonlinear processes (Huang et al., 1998; Wu and Huang, 2009). To date, EEMD has been widely applied in engineering, computer science, physics, and Earth and planetary sciences (Wu et al., 2008; He et al., 2014; Qiao et al., 2016; Zhang et al., 2018; Zhang et al., 2022).

In this work, direct measurements of two key GHGs, CH_4 and CO_2, along with $PM_{2.5}$ (particulate matter with an aerodynamic diameter ⩽ 2.5 μm) and TVOC (total volatile organic compound) concentrations, were carried out at the Bohe (BH) station on the northern South China Sea coast in Guangdong, China, during June 2021. The diurnal patterns of CH_4 and CO_2 during the SB/LB events were extracted and examined by EEMD. In addition, our observational results were compared with those of previous studies. Moreover, the influence of meteorological conditions and air pollutants on atmospheric CO_2 and CH_4 was further investigated to identify their possible sources.

2 Data and methodology

2.1 Sampling site and instruments

Sampling of atmospheric CH_4 and CO_2 concentrations was carried out in June 2021 at the sampling site in Bohe, Guangdong, China (21°27'N, 111°18'E, ~10 m a.s.l. (above sea level); Fig. 1). The BH station is located on the southern coast of the Liantou Peninsula in the northern SCS, which is far from urban areas and is without any surrounding vegetation or soil. In addition, this region is characterized by year-round warmth and humidity but with frequent disastrous weather events such as typhoons, strong winds, rainstorms and sea fogs (Huang and Chan, 2011), which arouses the interest of the public towards weather observations in this area.

The sampling site was equipped with a small-sized sampling container with an air conditioner. In the sampling container, a Fast Greenhouse Gas Analyser (GGA-30r-EP, Los Gatos Research, Inc., San Jose, CA, USA) and a handheld TVOC monitor (SDL511, Shandong Nova Fitness Co., Ltd., China) were installed for the simultaneous monitoring of GHGs together with relative air pollutants. During the sampling period, atmospheric CH_4 and CO_2 were simultaneously measured by the Fast Greenhouse Gas Analyser, which provided continuous measurements of CH_4 and CO_2 at a response rate of 10 Hz. Except for the internal filter, there were two external filters placed in the air inlet and the inlet line near the instrument to avoid contamination from dust and water vapour, respectively (Zhang et al., 2017). The TVOC concentrations were monitored by a photoionization detector (PID) at a resolution of 1 minute. The $PM_{2.5}$ mass concentrations were monitored with the laser scattering method at a resolution of 5 minutes. Ambient air was drawn into the sampling container through a main tube and then into each analyser or monitor. To avoid potential condensation water in the sampling tube, an automatic heating dehumidification system was deployed in this study (Li et al., 2020). Our observations were conducted during the whole month in June 2021, and calibrations were strictly performed before and after sampling.

2.2 Data analysis method

In this study, we applied EEMD, an adaptive analysis method (Wu and Huang, 2009) to determine and analyse the time-varying diurnal patterns of CH_4 and CO_2. EEMD was developed based on empirical mode decomposition (EMD) (Huang et al., 1998), which is a noise-assisted data analysis method to avoid the mode-mixing problem in the original EMD method. Detailed information can be found in Wu and Huang (2009).

The CH_4 and CO_2 timeseries $x(t)$, can be decomposed into several amplitude-frequency modulated oscillatory components (intrinsic mode functions, *IMFs*) from high-frequency to low-frequency timescales and a residue trend R_n given as (Eq. (1)):

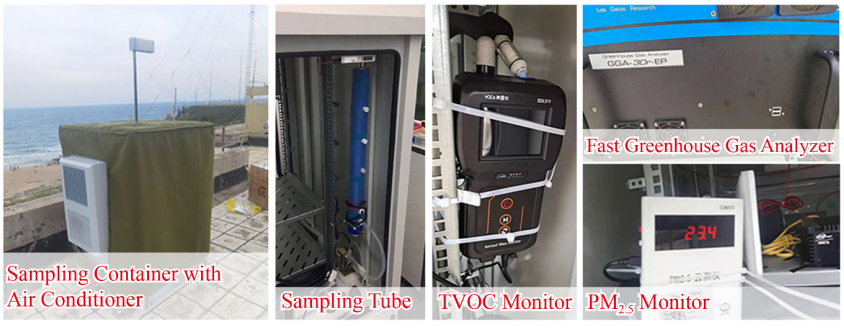

Fig. 1 Main sampling devices in the sampling container.

$$x(t) = \sum_{i=1}^{n} IMF\,s_i(t) + R_n(t), \quad (1)$$

where, the number of *IMFs*(n) is determined by the length of the data (N), which is defined as $\log_2(N) - 1$. The main decomposed procedures are given as:

1) To avoid the drawback of mode mixing in the original EMD method, we followed the method of Wu and Huang (2009) by adding white noise series into the CH_4 or CO_2 data;

2) The data together with the added white noise were decomposed into *IMFs*;

3) Step 1) and 2) were repeated a certain number of times with different white noises each time; and

4) The ensemble means of the corresponding *IMFs* from high-frequency to low-frequency timescales were obtained as the final result; meanwhile, the means of the corresponding *IMFs* of different white noise series likely cancelled each other without a real contribution to the *IMFs* of the data.

EEMD has been widely acknowledged for its ability to extract physical information effectively from nonlinear and nonstationary signals (Wu et al., 2008; Chen et al., 2013; Zhang et al., 2022), since it is similar to peeling an onion layer by layer without any previously determined basis functions. The advantages of using EEMD to extract the modulated annual cycle, with both frequency and amplitude time-varying, from a climate variable, have been validated by analysing synthetic datasets (Wu et al., 2008). Following the concept of a modulated annual cycle proposed by Wu et al. (2008), the extracted modulated diurnal cycle (MDC) by EEMD in this study, with a frequency of approximately 24 h, would allow us to examine the day-to-day variations in the diurnal pattern; hence, it could present precise diurnal variations, as it is time-varying in both frequency and amplitude. Introducing the MDC in atmospheric chemistry studies can improve the understandings of the shifting trends in daily variations and their causes.

3 Results and discussion

3.1 CH_4 and CO_2 timeseries and their comparisons with previous studies

In situ measurements of atmospheric CH_4, CO_2 and meteorological parameters were conducted at the BH station for the whole month in June 2021 (Fig. 2). CH_4 and CO_2 showed distinctly different patterns with changes in wind directions. According to the location of the BH station and the orientation of the coastline, the south and north winds are referred to as the SB and LB events, respectively. The whole month observational datasets were separated into three episodes according to wind directions. Episode 1 (E1) (6–11 June 2021) and Episode 3 (E3) (21–26 June) represent the LB events, and Episode 2 (E2) (15–21 and 26–30 June) represents the SB

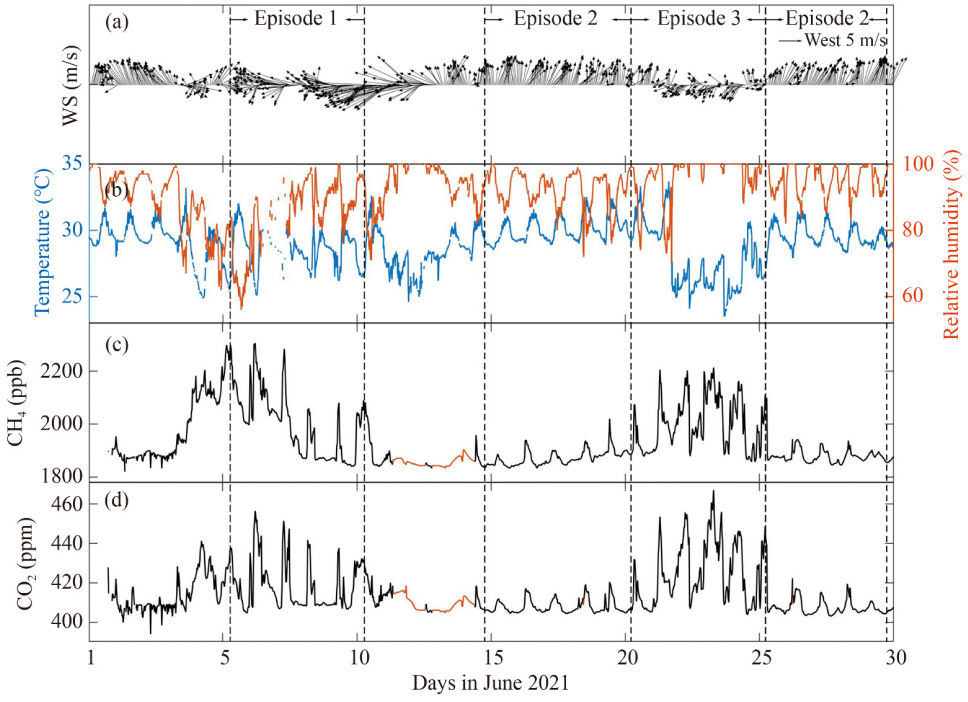

Fig. 2 (a) Time series of wind speed/direction, (b) air temperature and relative humidity, and (c) CH_4 and (d) CO_2 concentrations at the Bohe station in June 2021, segmented into Episode 1, Episode 2 and Episode 3 according to wind directions/speeds in June 2021. Data gaps of CH_4 and CO_2 during 12–15 June are interpolated, which are indicated by red lines (c, d).

events. Episodes 1 and 3 are further discerned by wind speeds (WS), relative humidity and temperature (Figs. 2(a) and 2(b)). Due to the CH_4 and CO_2 data scarcity before 5 June, we focused on the data analysis for the period during 6–30 June. The missing values during the power failure from 12–15 June were interpolated by the 24-h moving average (red lines in Figs. 2(c) and 2(d)) for further EEMD analysis.

The average concentrations of CH_4 and CO_2 during the SB events in June 2021 were 1876.91 ± 31.13 ppb and 407.99 ± 4.24 ppm, respectively, while they were 1988.12 ± 109.92 ppb and 421.54 ± 14.89 ppm during the LB events, respectively. The CH_4 and CO_2 concentrations during the SB and LB events in this study were consistent with measurements conducted at other onshore sites and offshore sites, respectively (Table 1). Figure 3 also presents a comparison of the CH_4 and CO_2 concentrations during the past 10 years at a series of observational sites from previous studies and our observational values at the BH site during the SB events. Among these sampling sites, the Mauna Loa in Hawaii, USA, and Mt. Waliguan in Qinghai, China, are the WMO/GAW baseline sites, representing the background conditions of the Pacific Ocean and the Asia continent, respectively. Dongsha Island and Yongxing Island are two islands in the SCS, while Hok Tsui and King's Park are located in Hong Kong, China. From these observations, the ever-increasing concentrations of atmospheric CH_4 and CO_2 in June for the past 10 years were determined. The CH_4 concentrations observed during June 2021 under the SB conditions at the BH station were similar to those at the Mauna Loa but lower than those at Mt. Waliguan and slightly higher than those on Dongsha Island in June in recent years (Fig. 3(a)). Compared with CO_2 values at other sites shown in Fig. 3(b), CO_2 values during the SB events at the BH station were consistent with the records at sites in Hok Tsui and King's Park but slightly lower than others, which might suggest stronger anthropogenic impacts in coastal areas than in the open oceans and in offshore areas. Combining Table 1 and Fig. 3, the values of CH_4 and CO_2 at the BH station basically coincided with previous measurements, which were consistent with the general trends reported in previous studies, as expected. This indicates that the observations of GHGs at the BH station could represent the background levels during the SB events and could be appropriate for long-term atmospheric GHG monitoring and further dynamics analysis. In addition, the GHG observation network in the SCS would be an important addition to globally undersampled coastal regions.

3.2 Diurnal patterns of CH_4 and CO_2

Based on the original time series shown in Fig. 2, all parameters showed significant diurnal variations. In contrast to the traditional methods that take the average values as the diurnal variations, we used EEMD to decompose the original data (half-hourly average CH_4 and CO_2 concentrations and wind speeds) into a number of *IMFs* from high-frequency to low-frequency timescales and residual trends (Figs. 4(a)–4(c)). The extracted components with a quasi-diurnal period (*IMF3s* in Figs. 4(a)–4(c)) are called the modulated diurnal cycle (MDC), in which amplitude and frequency vary with time. The proportions of the extracted MDC were determined as the ratios of the standard deviations of the MDC to the total standard deviations of all *IMFs*, which were approximately 26%, 29% and 22% for CH_4, CO_2 and WS, respectively (Fig. 4(d)). The interpolated part during 12–15 June did not show any diurnal pattern due to the procedure of 24-h moving average interpolation; moreover, this confirmed that the EEMD method used in

Table 1 Comparison of atmospheric CH_4 and CO_2 concentrations with previous studies. (Note: The NOAA/ESRL and the SIO refer to the NOAA Earth System Research Laboratory and the Scripps Institution of Oceanography)

Observational Site	Observational Period	CH_4 (ppb)	CO_2 (ppm)	Reference
Bohe, Guangdong, China	Jun. 2021 (during SB)	1876.91 ± 31.13	407.99 ± 4.24	This study
Bohe, Guangdong, China	Jun. 2021 (during LB)	1988.12 ± 109.92	421.54 ± 14.89	This study
Northern Yellow Sea and Bohai Strait, China	Jul. 2011	1823.8–2020.7	/	Zang et al., 2013
Northern Yellow Sea and Bohai Strait, China	May. 2012	1887.2–2136.2	/	Zang et al., 2013
Greenland, Denmark	Jul. 2012	1720–1880	/	Webster et al., 2015
Yongxing Island, China	Dec. 2013–Nov. 2014	/	399.12–405.39	Lv et al., 2015
Yongxing Island, China	Dec. 2013–Nov. 2017	1797–1944	/	Jiang et al., 2021
Thumba, Thiruvananthapuram, India	Jan. 2014–Aug. 2016	1989–2022	/	Kavitha et al., 2018
Pudong, Shanghai, China	Jun. 2017–May. 2018	2154 ± 190	428.36 ± 13.96	Wei et al., 2019
Mt. Waliguan, Qinghai, China	2019	1932.0 ± 0.1	/	Liu et al., 2021
Mauna Loa, Hawaii, USA	Sept. 2021	/	413.3	NOAA/ESRL and SIO
Global annual mean	2018	1869 ± 2	407.8 ± 0.1	World Meteorological Organization, 2019
Global annual mean	2019	1877 ± 2	410.5 ± 0.2	World Meteorological Organization, 2020

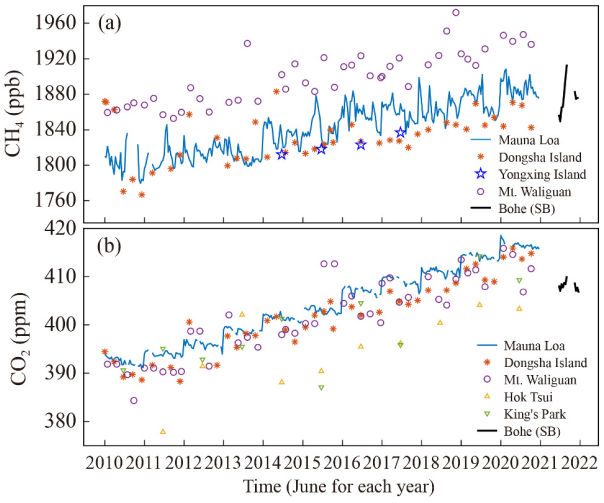

Fig. 3 (a) Comparison of CH_4 and (b) CO_2 concentrations observed in this study (black line during sea breeze) with previous studies (coloured lines, dots and stars), with all values observed in June for each year. The greenhouse gas data at the Mauna Loa, Dongsha Island and Mt. Waliguan are from the website of the NOAA Global Monitoring Laboratory Carbon Cycle Cooperative Global Air Sampling Network. The CO_2 data in Hok Tsui and King's Park are updated online from the World Data Centre for Greenhouse Gases (WDCGG) website provided by the Hong Kong Observatory (China), while the CH_4 data on Yongxing Island are from Jiang et al. (2021).

this study could effectively extract the signals at different timescales even with the artificially interpolated signals in the original time series. The amplitudes of the diurnal variations in CH_4 and CO_2 during the LB events (E1 and E3 in Fig. 4(d)) were almost two to three times those during the SB events (E2 in Fig. 4(d)).

A detailed examination of the changes in amplitude and frequency of diurnal patterns is shown in Fig. 5. For both CH_4 and CO_2, compared with the amplitude in E2 during the SB events, the amplitudes doubled or even tripled during the LB episodes (E1 and E3). One key feature was that a large discrepancy existed in the frequency for the peak times. For E1 and E3 during the LB events, the peak times of CH_4 and CO_2 occurred at 5:00–7:00 local time, with the minimum values recorded at approximately 18:00–20:00 local time (Figs. 5(a) and 5(b)). Thus, during the LB episodes, the diurnal patterns for CH_4 and CO_2 were generally characterized by a decrease after sunrise and an increase after sunset, which coincided with the values of previous studies at both onshore sites and offshore sites, mainly due to the diurnal variations in the BLH (Kavitha et al., 2018; Wei et al., 2019; Dimitriou et al., 2021). For E2, the times to peaks and troughs of diurnal variations in CH_4 and CO_2 occurred at approximately 9:00 and 18:00–22:00 local time, respectively, with peak times approximately 2 h to 4 h later than those during the LB events (Figs. 5(a) and 5(b)). The mid-morning high and evening low patterns for CH_4 and CO_2 in E2 were obviously different from those in E1 and E3, as well as from previous studies reported in the SCS (Lv et al., 2015; Jiang et al., 2021). Comprehensively, the diurnal patterns of CH_4 and CO_2 displayed an inverse relationship with diurnal variations in WS (Fig. 5(c)). Notably, the wind speed in E2 maintained its minimum values for at least four hours from 6:00–10:00, and its peak values lagged approximately 2 h compared with the LB episodes. This may possibly explain the phase lags in diurnal variations in CH_4 and CO_2 during the SB events. Our results show that the diurnal patterns of CH_4 and CO_2 were strongly correlated with winds in both amplitude

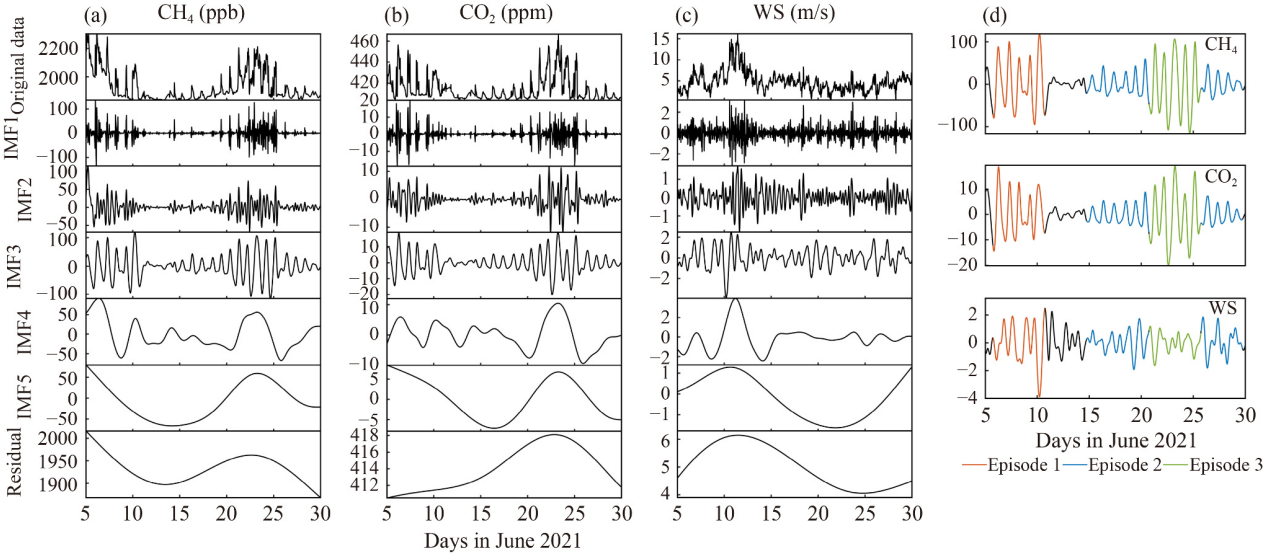

Fig. 4 (a) Time series of atmospheric CH_4 and (b) CO_2 concentrations and (c) wind speed, with their extracted components from high-frequency to low-frequency using EEMD. (d) The *IMF3s* represent the diurnal fluctuations, segmented into Episode 1 (orange), Episode 2 (blue) and Episode 3 (green) at the Bohe station during June 2021.

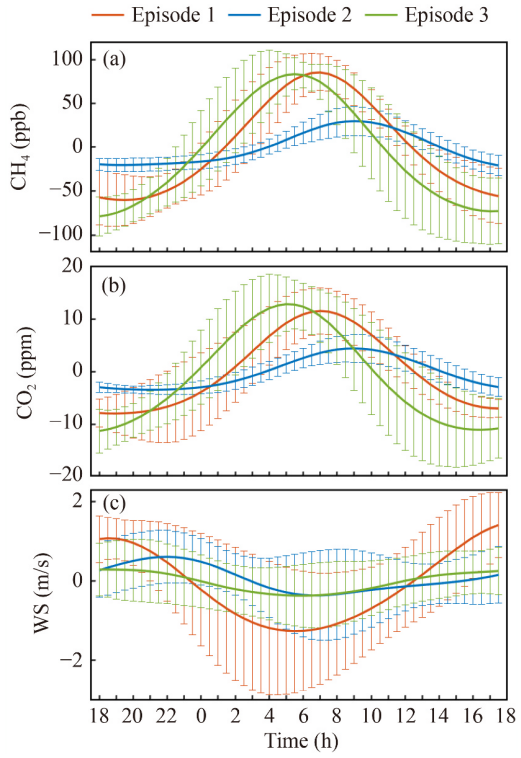

Fig. 5 Comparison of diurnal variations in (a) CH_4, (b) CO_2 and (c) wind speed as observed during Episode 1 (orange), Episode 2 (blue) and Episode 3 (green) at the Bohe station. Error bars indicate standard deviations with confidence intervals of 95%.

and phase. The relationship between GHG concentrations and their variations during LB/SB events has occasionally been considered in previous studies. Kavitha et al. (2018) studied diurnal variations in atmospheric CH_4 in Thumba, India, a tropical coastal station and found that the changes in the diurnal patterns of CH_4 were closely associated with the LB/SB events. However, the relationship between GHG concentrations and meteorological parameters has scarcely been addressed to date (Pérez et al., 2019), and how diurnal patterns of CH_4 and CO_2 change in detail with changing synoptic meteorology at coastal stations also needs further investigation.

3.3 Influence of meteorological conditions and atmospheric pollutants

The source attribution of CH_4 and CO_2 at the BH station was further investigated by combining wind speeds/directions and related air pollutants ($PM_{2.5}$ and TVOCs) (Figs. 6 and 7). As proven in Figs. 1 and 4, wind direction was the most important factor affecting CH_4 and CO_2 concentrations. However, less correlation between GHGs and wind speed can be found. For E1 and E3, when wind speeds were below 8 m/s, GHGs exhibited high concentration levels because both CH_4 and CO_2 emitted from local sources were accumulated (Figs. 6(a) and 6(b)). While for wind speeds above 8 m/s, for most cases in E1 and E3, both CH_4 and CO_2 remained at low levels. For E2, both CH_4 and CO_2 concentrations remained relatively stable with changes in wind speeds, which showed slightly negative correlations ($-0.4 < r < -0.2$), suggesting that background levels of CH_4 and CO_2 can be measured during the SB events at our observational site. However, the sporadically high concentrations of CH_4 and CO_2 in E2 were probably attributable to local accumulation from GHG emissions at low wind speeds. For wind speeds above 5 m/s and below 5 m/s, CH_4 and CO_2 showed moderately positive ($0.3 < r < 0.5$) and very weak negative correlations ($-0.2 < r < 0$) with TVOCs for E1 and E3, respectively (Figs. 6(c) and 6(d)). Given that the BH station was a coastal station far from the urban site, the positive correlation between GHGs and TVOCs for E1 was probably attributed to the long-range transport of air pollutants from urban areas. Moreover, slightly negative correlations ($-0.4 < r < -0.2$) between GHGs (CH_4 and CO_2) and TVOCs for E2 was determined, maintaining the background scope regardless of changes in TVOC concentrations. For the correlations between GHGs (CH_4 and CO_2) and $PM_{2.5}$, both CH_4 and CO_2 had positive correlations with $PM_{2.5}$ concentrations ($0.3 < r < 0.9$) under LB situations (Figs. 6(e) and 6(f)). In addition, under SB situations, CH_4 showed a positive correlation with $PM_{2.5}$, and the correlation between CO_2 and $PM_{2.5}$ can be negligible (Figs. 6(e) and 6(f)). This indicates that compared with CO_2, CH_4 emissions and transport showed a stronger correlation and proved more sensitive to air particulate matter at the BH station.

To further clarify the possible sources of CH_4 and CO_2, as well as correlated air pollutants ($PM_{2.5}$ and TVOCs), we present the bivariate polar plot analysis separately for all observed components with wind speeds/directions during the entire sampling period (Fig. 7). Bivariate plots were proven to be an efficient method for source detection by combining wind speed/direction, with the code obtained from the openair package in the R software (Carslaw and Beevers, 2013). High CH_4, CO_2 and $PM_{2.5}$ concentrations appeared consistently under low wind speeds (< 7 m/s) from the north (Figs. 7(a)–7(c)). This indicates that local sources of CH_4, CO_2 and $PM_{2.5}$ existed. Relatively high concentrations of CH_4 and CO_2 were also observed under high wind speeds (> 7 m/s) from both the northwest and northeast, attributed to atmospheric transport from the neighbouring sites. In particular, background levels of CH_4 and CO_2 were from the south winds (the sea breeze directions), mainly due to the clear air from the ocean, which diluted and decreased the concentrations of CH_4 and CO_2. Comparatively, high TVOC concentrations occurred both under low wind speeds from the south and high wind speeds from the northeast, indicating that the ocean is one of the important natural sources of TVOCs (Fig. 7(d)). Furthermore, the wetlands and continental shelves south (including southeast and southwest) of the observational site are also probably natural sources.

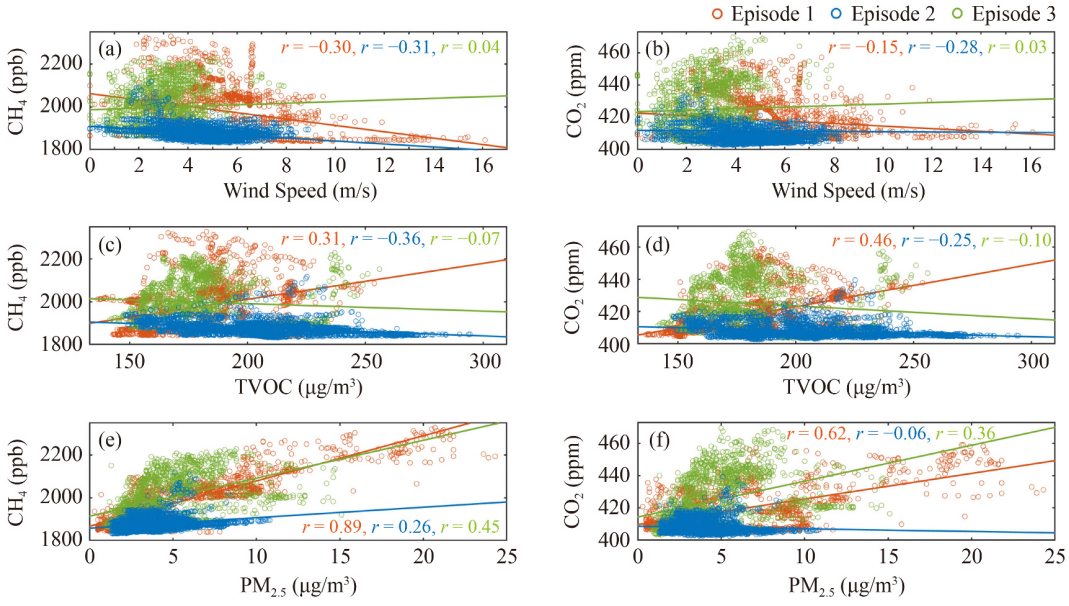

Fig. 6 Scatterplots of CH_4 and CO_2 concentrations versus (a, b) wind speed, (c, d) TVOCs and (e, f) $PM_{2.5}$ for three episodes. Fitted lines of the corresponding colored circles represent the ordinary least-squared regression model, and r is the Pearson Correlation Coefficient.

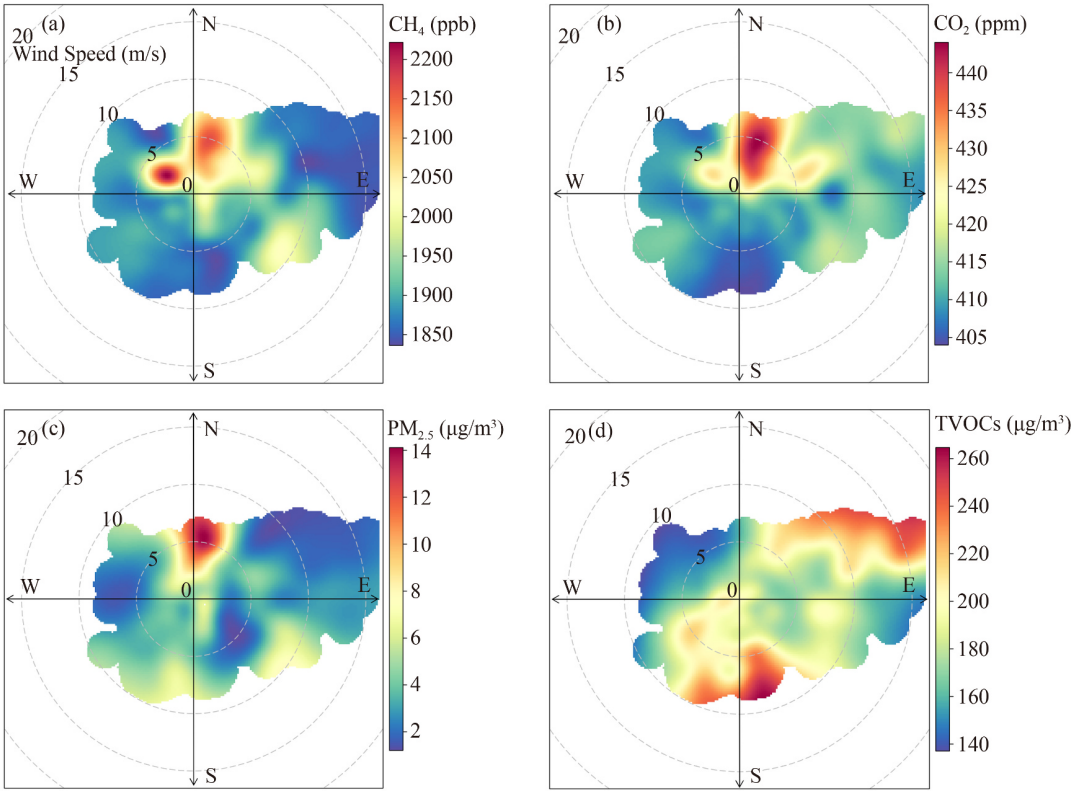

Fig. 7 Bivariate polar plots for (a) CH_4, (b) CO_2, (c) $PM_{2.5}$ and (d) TVOCs concentrations at the Bohe station in June 2021.

Combining the correlation and bivariate plot analyses (Figs. 6 and 7), wind speeds/directions significantly modulated the CH_4 and CO_2 levels at our observational site. In addition, both TVOCs and $PM_{2.5}$ modulated CH_4 and CO_2, associated with the synchronized sources and transport processes. Given the concern about these processes and the potential for CH_4 to generate ground-level ozone that is harmful to human health, reduction of

the emissions of CH_4 and CO_2 together with air pollutants has extreme significance (Wei et al., 2019). Isotope tracers such as ethane should be considered in future observations to further discern the proportions of natural and anthropogenic sources of CH_4 (Brandt et al., 2014).

4 Conclusions

This study presents the first measurements of atmospheric CH_4 and CO_2 concentrations that were conducted at the BH station in the northern SCS in June 2021. The diurnal patterns of CH_4 and CO_2 at the BH station were extracted based on EEMD and were further analysed with meteorological parameters and air pollutants to further identify the possible sources of CH_4 and CO_2.

The average CH_4 and CO_2 concentrations at the BH station were 1876.91 ± 31.13 ppb and 407.99 ± 4.24 ppm during the SB events, and 1988.12 ± 109.92 ppb and 421.54 ± 14.89 ppm during the LB events, respectively. The values of CH_4 and CO_2 measured during the SB events at the BH station basically coincided with the values and trends of marine background sites.

With the help of EEMD, time-varying diurnal variations in CH_4 and CO_2 were clearly extracted, which accounted for approximately 26% and 29% of all extracted components except the residual trends, respectively. The amplitudes of the diurnal variations in CH_4 and CO_2 during the LB events were two to three times those during the SB events. In addition, the diurnal variations in CH_4 and CO_2 during the LB events showed sunrise high and sunset low patterns with peaks at 5:00–7:00; however, the diurnal patterns for CH_4 and CO_2 during the SB events showed mid-morning high and evening low with peaks at approximately 9:00 (obviously 2 h to 4 h later than that during the LB events). Comprehensively, noticeable differences in the amplitude and phase of diurnal variations in CH_4 and CO_2 during the LB/SB events were probably attributed to diurnal patterns of wind speeds during the LB/SB episodes.

Comprehensively, wind directions played a significant role in the CH_4 and CO_2 levels at the BH site. Elevated concentrations of CH_4 and CO_2 appeared in stable wind conditions, probably associated with local accumulation from GHG emission sources, as well as the long-range transport from remote sources by winds under high speeds from the northwest and northeast. In contrast, background levels of CH_4 and CO_2 were observed from the south winds, mainly due to the clear air from the ocean. Aside from meteorological parameters, air pollutants such as TVOCs and $PM_{2.5}$ also modulated CH_4 and CO_2 due to the synchronized sources and transport, which presented extreme conditions for reducing the emissions of GHGs together with air pollutants.

The observational parameters and duration were limited in this study, and we are eager to perform comprehensive measurements that focus on the diurnal patterns of GHGs in the SCS in the near future. Our results demonstrate that the BH station can serve as an ideal site for long-term GHG monitoring and dynamics analysis. Future analysis will benefit from ongoing observations at the BH station.

Acknowledgements This work was supported by the Basic Scientific Fund for National Public Research Institutes of China (No. 2018Q01), the Natural Science Foundation of Shandong Province (China) (No. ZR202102190358), the National Natural Science Foundation of China (No. 41821004), the international cooperation project on Indo-Pacific Ocean environmental variability and air-sea interactions (China) (No. GASI-IPOVAI-05), and the Aoshan Talents Cultivation Excellent Scholar Program supported by Qingdao National Laboratory for Marine Science and Technology (China) (No. 2017ASTCP-ES04).

Conflict of Interest The authors declare that they have no conflicts of interest.

References

Bai Y N, Wang X N, Zhang F, Zeng R J (2022). Acid Orange 7 degradation using methane as the sole carbon source and electron donor. Frontiers of Environmental Science & Engineering, 16(3): 34

Brandt A R, Heath G A, Kort E A, O'Sullivan F, Pétron G, Jordaan S M, Tans P, Wilcox J, Gopstein A M, Arent D, Wofsy S, Brown N J, Bradley R, Stucky G D, Eardley D, Harriss R (2014). Methane leaks from North American natural gas systems. Science, 343(6172): 733–735

Cai W J, Dai M H, Wang Y C (2006). Air-sea exchange of carbon dioxide in ocean margins: A province-based synthesis. Geophysical Research Letters, 33(12): L12603

Canadell J G, Monteiro P M S, Costa M H, Cotrim da Cunha L, Cox P M, Eliseev A V, Henson S, Ishii M, Jaccard S, Koven C, et al. (2021). Global carbon and other biogeochemical cycles and feedbacks. In: Masson-Delmotte V, Zhai P, Pirani A, Connors S L, Péan C, Berger S, Caud N, Chen Y, Goldfarb L, Gomis M I, et al., eds. Climate Change 2021: The Physical Science Basis. Contribution of Working Group I to the Sixth Assessment Report of the Intergovernmental Panel on Climate Change. Cambridge: Cambridge University Press

Carslaw D C, Beevers S D (2013). Characterising and understanding emission sources using bivariate polar plots and k-means clustering. Environmental Modelling & Software, 40: 325–329

Chen X Y, Zhang Y L, Zhang M, Feng Y, Wu Z H, Qiao F L, Huang N E (2013). Intercomparison between observed and simulated variability in global ocean heat content using empirical mode decomposition, part I: modulated annual cycle. Climate Dynamics, 41(11−12): 2797–2815

Clow J, Smith J C (2016). Using Unmanned Air Systems to Monitor Methane in the Atmosphere. NASA/TM–2016–219008. Hampton: Langley Research Center

Coumou D, Rahmstorf S (2012). A decade of weather extremes. Nature Climate Change, 2(7): 491–496

Diffenbaugh N S, Singh D, Mankin J S, Horton D E, Swain D L, Touma D, Charland A, Liu Y J, Haugen M, Tsiang M, Rajaratnam

B (2016). Quantifying the influence of global warming on unprecedented extreme climate events. Proceedings of the National Academy of Sciences, 114(19): 4881–4886

Dimitriou K, Bougiatioti A, Ramonet M, Pierros F, Michalopoulos P, Liakakou E, Solomos S, Quehe P Y, Delmotte M, Gerasopoulos E, et al. (2021). Greenhouse gases (CO_2 and CH_4) at an urban background site in Athens, Greece: Levels, sources and impact of atmospheric circulation. Atmospheric Environment, 253(6): 118372

Dlugokencky E J, Nisbet E G, Fisher R, Lowry D (2011). Global atmospheric methane: Budget, changes and dangers. Philosophical Transactions. Series A, Mathematical, physical, and engineering sciences, 369(1943): 2058−2072

Fang S X, Tans P P, Yao B, Luan T, Wu Y L, Yu D J (2017). Study of atmospheric CO_2 and CH_4 at Longfengshan WMO/GAW regional station: The variations, trends, influence of local sources/sinks, and transport. Science China. Earth Sciences, 60(10): 1886–1895

Forster P, Storelvmo T, Armour K, Collins W, Dufresne J L, Frame D, Lunt D J, Mauritsen T, Palmer M D, Watanabe M, et al. (2021). The Earth's energy budget, climate feedbacks, and climate sensitivity. In: Masson-Delmotte V, Zhai P, Pirani A, Connors S L, Péan C, Berger S, Caud N, Chen Y, Goldfarb L, Gomis M I, et al., eds. Climate Change 2021: The Physical Science Basis. Contribution of Working Group I to the Sixth Assessment Report of the Intergovemmental Panel on Climate Change. Cambridge: Cambridge University Press

Gulev S K, Thorne P W, Ahn J, Dentener F J, Domingues C M, Gerland S, Gong D, Kaufman D S, Nnamchi H C, Quaas J, et al. (2021). Changing state of the climate system. In: Masson-Delmotte V, Zhai P, Pirani A, Connors S L, Péan C, Berger S, Caud N, Chen Y, Goldfarb L, Gomis M I, et al., eds. Climate Change 2021: The Physical Science Basis. Contribution of Working Group I to the Sixth Assessment Report of the Intergovernmental Panel on Climate Change. Cambridge: Cambridge University Press

He J J, Zhang M, Chen X Y, Wang M (2014). Inter-comparison of seasonal variability and nonlinear trend between AERONET aerosol optical depth and PM_{10} mass concentrations in Hong Kong (China). Science China. Earth Sciences, 57(11): 2606–2615

Huang J, Chan P W (2011). Progress of marine meteorological observation experiment at Maoming of South China. Journal of Tropical Meteorology, 17(4): 418–429

Huang N E, Zheng S, Long S R, Wu M C, Shih H H, Zheng Q, Yen N C, Tung C C, Liu H H (1998). The empirical mode decomposition and the Hilbert spectrum for nonlinear and non-stationary time series analysis. Philosophical Transactions. Series A, Mathematical, physical, and engineering sciences, 454(1971): 903–995

Ji X L, Liu G M, Gao S, Wang H, Zhang M Y (2017). Comparison of air-sea CO_2 flux and biological productivity in the South China Sea, East China Sea, and Yellow Sea: A three-dimensional physical-biogeochemical modeling study. Acta Oceanologica Sinica, 36(12): 1–10

Jiang Y F, Wang X Q, Wang H Y, Xu Y S, Lv H G (2021). Study on the concentration variation and impact factors of CH_4 in Yongxing Island. China Environmental Science, 41(11): 5054−5059 (in Chinese)

Kavitha M, Nair P R, Girach I A, Aneesh S, Sijikumar S, Renju R (2018). Diurnal and seasonal variations in surface methane at a tropical coastal station: Role of mesoscale meteorology. Science of the Total Environment, 631–632: 1472–1485

Kong S F, Lu B, Han B, Bai Z P, Xu Z, You Y, Jin L M, Guo X Y, Wang R (2010). Seasonal variation analysis of atmospheric CH_4, N_2O and CO_2 in Tianjin offshore area. Science China. Earth Sciences, 53(8): 1205–1215

Li H Y, Zhu Y J, Zhao Y, Chen T S, Jiang Y, Shan Y, Liu Y H, Mu J S, Yin X K, Wu D, et al. (2020). Evaluation of the performance of low-cost air quality sensors at a high mountain station with complex meteorological conditions. Atmosphere, 11(2): 212

Li Q, Gogo S, Leroy F, Guimbaud C, Laggoun-Défarge F (2021). Response of peatland CO_2 and CH_4 fluxes to experimental warming and the carbon balance. Frontiers of Earth Science, 9: 631368

Liu S, Fang S X, Liu P, Liang M, Guo M R, Feng Z Z (2021). Measurement report: Changing characteristics of atmospheric CH_4 in the Tibetan Plateau: Records from 1994 to 2019 at the Mount Waliguan station. Atmospheric Chemistry and Physics, 21(1): 393–413

Lv H G, Wang H Y, Jiang Y F, Chen H N, Qiao R, Wang Z G (2015). Study on the concentration variation of CO_2 in the background area of Xisha. Acta Oceanologica Sinica, 37(6): 21−30 (in Chinese)

Pérez I A, Sánchez M L, García M Á, Pardo N (2019). Sensitivity of CO_2 and CH_4 annual cycles to different meteorological variables at a rural site in Northern Spain. Advances in Meteorology, 2019: 9240568

Qiao F L, Yuan Y L, Deng J, Dai D J, Song Z Y (2016). Wave-turbulence interaction-induced vertical mixing and its effects in ocean and climate models. Philosophical Transactions. Series A, Mathematical, Physical, and Engineering Sciences, 374(2065): 2015.201

Qu T D, Song Y T, Yamagata T (2009). An introduction to the South China Sea throughflow: Its dynamics, variability, and application for climate. Dynamics of Atmospheres and Oceans, 47(1−3): 3–14

Saunois M, Bousquet P, Poulter B, Peregon A, Ciais P, Canadell J G, Dlugokencky E J, Etiope G, Bastviken D, Houweling S, et al. (2016). The global methane budget 2000–2012. Earth System Science Data, 8: 697–751

Srivastava S, Lal S, Subrahamanyam D B, Gupta S, Venkataramani S, Rajesh T A (2010). Seasonal variability in mixed layer height and its impact on trace gas distribution over a tropical urban site: Ahmedabad. Atmospheric Research, 96(1): 79–87

Thomas G, Zachariah E J (2012). Ground level volume mixing ratio of methane in a tropical coastal city. Environmental Monitoring and Assessment, 184(4): 1857–1863

United Nations Environment Programme (2021). Global Methane Assessment: Benefits and Costs of Mitigating Methane Emissions. Nairobi: United Nations Environment Programme

Webster K D, White J R, Pratt L M (2015). Ground-level concentrations of atmospheric methane in southwest Greenland evaluated using open-path laser spectroscopy and cavity-enhanced absorption spectroscopy. Arctic, Antarctic, and Alpine Research, 47(4): 599−609

Wei C, Wang M H, Fu Q Y, Dai C, Huang R, Bao Q (2019). Temporal characteristics of greenhouse gases (CO_2 and CH_4) in the megacity Shanghai, China: Association with air pollutants and meteorological conditions. Atmospheric Research, 235: 104759

World Meteorological Organization (2019). Greenhouse Gas Bulletin: The State of Greenhouse Gases in the Atmosphere Based on Global Observations through 2018. Geneva: World Meteorological Organization

World Meteorological Organization (2020). Greenhouse Gas Bulletin: The State of Greenhouse Gases in the Atmosphere Based on Global Observations through 2019. Geneva: World Meteorological Organization

Wu Z H, Huang N E (2009). Ensemble empirical mode decomposition: A noise-assisted data analysis method. Advances in Adaptive Data Analysis, 1(01): 1–41

Wu Z H, Schneider E K, Kirtman B P, Sarachik E S, Huang N E, Tucker C J (2008). The modulated annual cycle: An alternative reference frame for climate anomalies. Climate Dynamics, 31(7): 823–841

Zang K P, Zhao H D, Wang J Y, Xu X M, Huo C, Zheng N (2013). High-resolution measurement of CH_4 in sea surface air based on cavity ring-down spectroscopy technique: The first trial in China Seas. Acta Scientiae Circumstantiae, 33(5): 1362−1366 (in Chinese)

Zhang K, Xu J L, Huang Q, Zhou L, Fu Q Y, Duan Y S, Xiu G L (2020). Precursors and potential sources of ground-level ozone in suburban Shanghai. Frontiers of Environmental Science & Engineering, 14(6): 92

Zhang M, Cheng Y Y, Bao Y, Zhao C, Wang G, Zhang Y L, Song Z Y, Wu Z H, Qiao F L (2022). Seasonal to decadal spatiotemporal variations of the global ocean carbon sink. Global Change Biology, 28(5): 1786–1797

Zhang M, Qiao F L, Song Z Y (2017). Observation of atmospheric methane in the Arctic Ocean up to 87ºN. Science China. Earth Sciences, 60(1): 173–179

Zhang M, Wu Z H, Qiao F L (2018). Deep Atlantic Ocean warming facilitated by the deep western boundary current and equatorial Kelvin waves. Journal of Climate, 31(20): 8541–8555

Zhang Y, Xiong X Z, Tao J H, Yu C, Zou M M, Su L, Chen L F (2014). Methane retrieval from atmospheric infrared sounder using EOF-based regression algorithm and its validation. Chinese Science Bulletin, 59(14): 1508–1518